Astronomy Letters, Vol. 27, No. 1, 2001, pp. 15–24. Translated from Pis'ma v Astronomicheskiĭ Zhurnal, Vol. 27, No. 1, 2001, pp. 19–30.

A Chemically Decoupled Nucleus and Structure of the Nuclear Region in the S0 Galaxy NGC 4036[¶]

O. K. Sil'chenko[1] * and V. V. Vlasyuk[2]

[1] *Sternberg Astronomical Institute, Universitetskiĭ pr. 13, Moscow, 119899 Russia*
[2] *Special Astrophysical Observatory, Russian Academy of Sciences, Nizhniĭ Arkhyz, Stavropolskiĭ Kraĭ, 357147 Russia*
Received February 2, 2000

Abstract—We present the results of a comprehensive spectrophotometric study of the central region in the regular lenticular galaxy NGC 4036 with two spectrographs of the 6-m telescope. The unresolved nucleus of NGC 4036 is shown to be chemically decoupled: [Mg/Fe] = +0.3 at the very center, whereas in the immediate vicinity of its nucleus, this ratio abruptly drops to +0.1 and does not change further along the radius. A study of isophotal morphology in combination with a kinematic analysis has proven that the rotation of stars at the NGC 4036 center is axisymmetric. However, the major-axis turn within $R < 5''$ should be considered real. We interpret this turn as evidence for the existence of a tilted circumnucelar stellar disk with a radius of ~250 pc in NGC 4036. The NGC 4036 bulge may be triaxial, and the ionized gas at the galactic center is then concentrated toward the principal plane of the ellipsoidal potential. © *2001 MAIK "Nauka/Interperiodica".*

Key words: *lenticular galaxies, circumnuclear stellar disks*

INTRODUCTION

Lenticular galaxies were judged by their evolutionary status and by the composition of their stellar population to be similar to ellipticals, i.e., old and devoid of any interstellar medium, as far back as twenty years ago. Now, as these galaxies are painstakingly studied, they prove to be increasingly complex systems. First of all, in contrast to ellipticals, more than 30% of them exhibit an appreciable amount of neutral hydrogen (Chamaraux *et al.* 1986). However, systematic searches for traces of star formation in the disks of lenticular galaxies with a sufficient amount of H I yielded negative results for most objects: no young stars capable of ionizing hydrogen were detected (Pogge and Eskridge 1987, 1993). Nevertheless, there is also ionized gas (or even it alone) in many lenticular galaxies. The ionized gas is generally concentrated in central regions and exhibits LINER excitation; it is thought to be either external in origin or have been ejected by bulge stars during their evolution (Bertola *et al.* 1992, 1995). Again, the presence of this gas is not accompanied by on-going star formation in the galactic nucleus; however, the stellar population of the nuclear regions in 50% of the lenticular galaxies was found to be younger than 5–7 Gyr (Sil'chenko 1993). Maybe this comparatively recent star formation is still associated with the acquirement of gas, for example, during the interaction with another galaxy. The structure of many lenticular galaxies turned out to be complex as well. A photometric study by Seifert and Scorza (1996) revealed two unrelated disks—outer extended and inner compact ones—in half of the lenticular galaxies from their sample (eight objects). Based on a detailed study, Van den Bosch and Emsellem (1998) diagnosed the same double-disk structure in the S0 galaxy NGC 4570. Can these two disks be formed at different evolutionary stages of the galaxy? In three objects (NGC 1023, 7280, and 7332), we managed to associate these photometrically identifiable circumnuclear stellar disks with regions distinguished by stellar-population properties, namely, by a heavy-element overabundance and a relatively young age, 2–5 Gyr (Sil'chenko 1999a; Afanas'ev and Sil'chenko 2000). At least, the circumnuclear compact stellar disks in these galaxies were formed during separate, relatively recent and fairly violent episodes of their evolution. Were these episodes related to the absorption of another galaxy? Do we see traces of mergers in lenticular galaxies, which, from a theoretical point of view, are most commonly attributed to the evolution of ellipticals, but which have not yet been reliably detected in regular galaxies?

NGC 4036 is a classical lenticular galaxy, which, being bright enough and nearby (its global parameters are given in Table 1), has repeatedly been investigated both photometrically and spectroscopically in various wavelength ranges. Kent (1984), Michard and Marchal (1993), and Cinzano *et al.* (1999) performed its CCD optical surface photometry. They all obtained roughly the same results: the galaxy has a regular radial brightness profile, which can be represented as the sum of an

[¶] Based on observations with the 6-m Special Astrophysical Observatory telescope.
* E-mail address for contacts: olga@sai.msu.ru

Table 1. Global parameters of NGC 4036 (LEDA database)

Morphological type	S0–
R_{25}	13 kpc
B_T^0	11.05
M_B	–20.63
$V_r(\odot)$	1392 km s^{-1}
V_r(LG)	1519 km s^{-1}
Distance	21.7 Mpc (H_0 = 75 km s^{-1} Mpc^{-1})
Disk inclination	71°
PA_{phot}	79°

extended exponential disk and a bright, but fairly compact de Vaucouleurs bulge. The optical rotation curve measured along the major axis of NGC 4036 both for the ionized gas and for stars by Fisher (1997), Bertola *et al.* (1995), and Cinzano *et al.* (1999) is closely similar for both galactic components and is also classical in shape: it rises virtually like a rigid-body one up to $R \approx$ 1 kpc and then flattens out. The velocity dispersions of the gas and stars within $R \approx 0.5$ kpc of the center are also the same, which led Cinzano *et al.* (1999) to conclude that the ionized gas at the NGC 4036 center originates in bulge stars. A radio study (Huchtmeier 1982) did not reveal any substantial amount of H I in the galaxy [note that Cinzano *et al.* (1999) committed an error in the Introduction to their paper: they took the upper limit on the H I mass in NGC 4036 from the catalog by Roberts *et al.* (1991) as the measured gas mass]. Thus, if there is a lenticular galaxy without any outward signs of the past interaction or merging, this is NGC 4036. Fisher *et al.* (1996) investigated the stellar population at the NGC 4036 center by measuring absorption-line indices (equivalent widths) in the integrated spectrum along the major and minor axes. Here, a peculiarity was first hinted at: they casually noted that an enhanced magnesium-to-iron ratio was observed in the galactic nucleus, which more closely resembles the stellar population of ellipticals, whereas the Mg/Fe ratio in the bulge is nearly solar. A simple visual analysis of their data argued for a chemically decoupled nucleus in NGC 4036. Since we have been investigating the chemically decoupled nuclei in disk galaxies [see Sil'chenko *et al.* (1992) for the discovery of such nuclei] and their possible origin through merging or interaction for several years, we have decided to carry out an independent spectroscopic study of NGC 4036.

OBSERVATIONS AND DATA REDUCTION

The central part of NGC 4036 was observed with a multipupil field spectrograph (MPFS) at the prime focus of the 6-m Special Astrophysical Observatory (SAO) telescope [see Afanas'ev *et al.* (1990) for a description of the instrument] three times: twice near the Mg Ib absorption line and once near Hα. In addition, we obtained one profile with a narrow 34″-long slit in the green using a spectrophotometric system at the Nasmyth-1 focus. A log of our spectroscopic observations for NGC 4036 is given in Table 2.

The detectors for the MPFS were Russian-made 520×580 and 1040×1160 CCD arrays; the spectrophotometric system at the Nasmyth-1 focus was equipped with a Photometrics 1024×1024 CCD. During the MPFS observations, an array of microlenses, 8×12 for the small CCD (in the red) and 8×16 for the large CCD (in the green), formed a pupil matrix, which was fed to the entrance of a grating spectrograph. This configuration allows up to 128 spectra to be simultaneously taken, each corresponding to a $1''.3 \times 1''.3$ spatial element of the galaxy image. We separately took a comparison spectrum of a helium–neon–argon lamp for wavelength calibration and a dawn-sky spectrum to make corrections for vignetting and for different microlens transmission. We also separately exposed the sky background near the galaxy in the green spectral range, where the equivalent widths of absorption lines were supposed to be calculated; its spectra were then smoothed and subtracted from the object's spectra. Since the sky background was not subtracted when reducing the long-slit spectrum (the slit was too short to "go" outside the galaxy), it was used to calculate absorption-line indices only in the immediate vicinity of the nucleus, where the galaxy is much brighter than the sky background. We calculated the velocities of the stellar component here by cross correlation with the dawn-sky spectrum. The main stages of data reduction—dark-current subtraction, cosmic-ray hit removal, extraction of one-dimensional spectra from the matrix format, extracted-spectrum linearization, construction of two-dimensional surface-brightness distributions and velocity fields—were performed by using the software package developed at the SAO (Vlasyuk 1993).

Table 2. Spectroscopic observations of NGC 4036

Date	T(exp), min	Field of view	PA(top)	Range, Å	Resolution, Å	$FWHM_*$
May 7, 1997	60	$10''.6 \times 21''.1$	221°	4100–5700	3.2–3.7	$2''.5$
Jan. 19, 1998	60	10.4×15.6	250	6200–6850	2.8–3.6	2.6
Jan. 23, 1998	40	10.9×21.8	67	4100–5700	4.0–5.5	2.2
Jan. 22, 1998	30	1.5×34	322	4500–5750	3.0	2.3

We used the MPFS observations in the spectral range 4100–5700 Å, first, to investigate the radial dependence of absorption-line equivalent widths and, second, to construct the two-dimensional line-of-sight velocity field of stars at the galactic center. The first goal was achieved by adding up the spectra in concentric rings centered on the galactic nucleus with a width and radial step of 1″.3, i.e., equal to the spatial element size; in this way, we managed to maintain an approximately constant signal-to-noise ratio along the radius, which is unattainable, say, during long-slit observations. Subsequently, we calculated the Hβ, Mgb, Fe5270, and Fe5335 indices in the standard Lick system (Worthey *et al.* 1994). Detailed model calculations in terms of synthesis models for an old stellar population are available for the above strong absorption lines (Worthey *et al.* 1994; Vazdekis *et al.* 1996; Tantalo *et al.* 1998). To achieve the second goal, the spectrum of each spatial element after continuum subtraction and conversion to the velocity scale was cross correlated with the spectra of the K0–K2 III giant stars observed during the set with the same instruments as the galaxy. The observations in the red were used to construct the two-dimensional ionized-gas line-of-sight velocity field. To this end, we measured precise centroid positions of the [N II] λ6583 emission line; since NGC 4036 is a LINER, the Hα emission is weak in its circumnuclear region. In addition, we constructed a surface-brightness map in [N II] λ6583 and in the nearby continuum. The night-sky λλ5577, 6300, and 6864 Å lines were used to check the wavelength-scale construction and the measured-velocity zero point. We estimated the accuracy of individual line-of-sight velocity measurements for the stars and the gas to be 20 and 30 km s^{-1}, respectively, and the accuracy of determining the equivalent widths of absorption lines in azimuthally averaged spectra to be 0.2 Å.

We made use of data from the Hubble Space Telescope (HST) archive to morphologically investigate the central part of NGC 4036. The galaxy was imaged with the WFPC2 instrument on August 8, 1994, as part of the Sargent Program "Searches for Active Galactic Nuclei of Very Low Luminosity." We used an F547M medium-band filter, which covered the spectral range from 5150 to 5800 Å; the exposure time was 300 s. The scale in the PC1 format with the galactic nucleus at its center was 0″.045 per pixel, and the spatial resolution was 0″.1. A 36″ × 36″ central part of the galaxy was exposed with this scale and resolution. The image morphology was analyzed with the FITELL code written by one of us (V.V.).

A CHEMICALLY DECOUPLED NUCLEUS IN NGC 4036

As we already mentioned in the Introduction, NGC 4036 belongs to those few lenticular galaxies whose circumnuclear stellar population has been studied by measuring absorption-line indices in the widely known Lick system. Fisher *et al.* (1996) carried out such a study in the one-dimensional case by observing NGC 4036 with a long slit along its major and minor axes. Jablonka *et al.* (1996) published similar "zero-dimensional" data: they integrated a 2″.5 × 10″.5 central region of the galaxy. We performed two-dimensional spectroscopy of NGC 4036 in the green twice and calculated an azimuthally averaged dependence of the Hβ, Mgb, Fe5270, and Fe5335 indices on distance to its center; we also have a one-dimensional profile of the galaxy with a long slit at position angle 142°, i.e., at 63° to the major axis. Figure 1 compares all our data with those of Fisher *et al.* (1996).

The first thing that catches the eye when looking at Fig. 1 is reasonably good agreement between all five observational sequences for the metal-line indices. This is a great stroke of luck, which could not be expected in advance: the Lick system of indices is believed to be fairly capricious and sensitive to the spectral resolution of observations. Meanwhile, our MPFS data with a resolution of 4–5 Å were reduced to the Lick system (resolution of ~8 Å) using the observations of standard

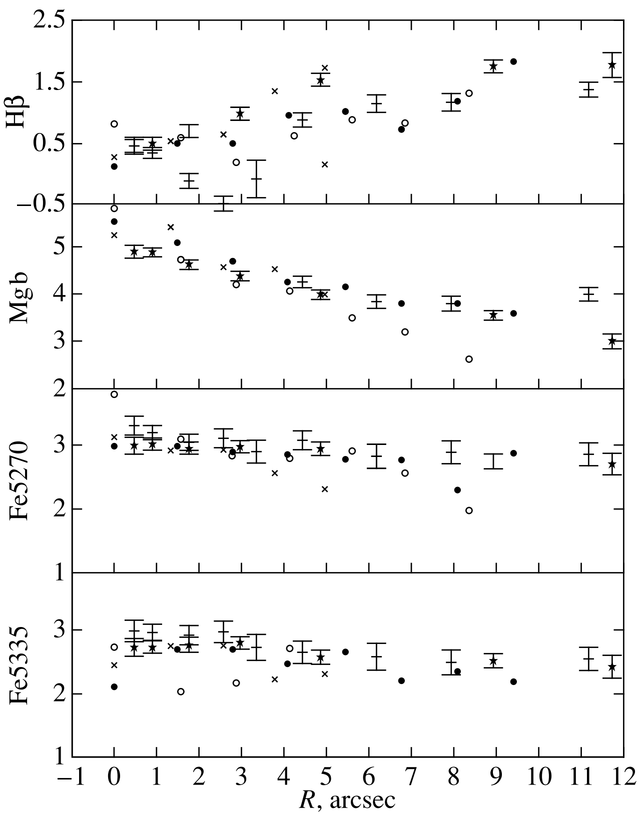

Fig. 1. Radial variations in Hβ, Mgb, Fe5270, and Fe5335 absorption-line indices, as inferred from our MPFS data in 1997 (dots) and 1998 (circles), from our long-slit data at Nasmyth-1 (crosses), and from the data of Fisher *et al.* (1996) obtained with a long slit along the major (pluses) and minor (asterisks) axes of NGC 4036. The measurements were corrected for stellar velocity dispersion in the galaxy.

Table 3. Mean absorption-line indices in the NGC 4036 nucleus

Hβ	0.40 ± 0.21
Mgb	5.56 ± 0.17
Fe5270	3.32 ± 0.26
Fe5335	2.44 ± 0.18

stars by Worthey *et al.* (1994), as were the data of Fisher *et al.* (1996), whereas no observations with the spectrophotometric system at Nasmyth-1 with 3 Å resolution are available. The absence of a systematic difference between the measured Mgb, Fe5270, and Fe5335 indices in the above papers proves that spectroscopic observations at Nasmyth-1 with such a spectral resolution and with stellar velocity dispersions in the galaxy of the order of 200 km s^{-1} yield the metal-line indices precisely in the Lick system and require no additional calibration. Yet another practical conclusion following from Fig. 1 is that the indices for the NGC 4036 nucleus can be estimated by directly averaging our three independent measurements. Mean estimates of the indices for the NGC 4036 nucleus with their errors corrected for a stellar velocity dispersion of 190 km s^{-1} [the mean between those given by Fisher (1997) and Chinzano *et al.* (1999)] are listed in Table 3.

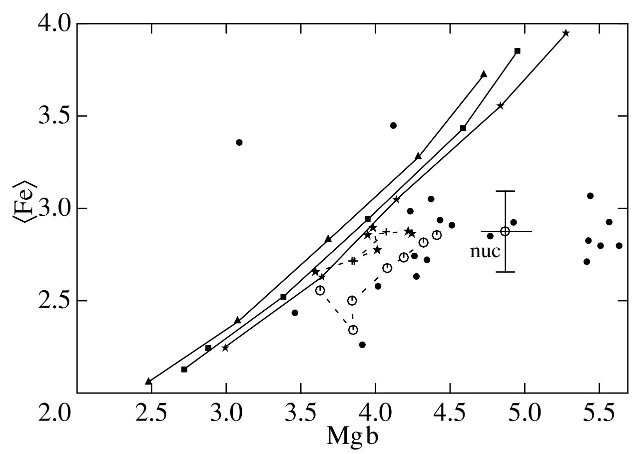

Fig. 2. (⟨Fe⟩, Mgb) diagram: a comparison of models and observational data. The models of Worthey (1994) (solid lines) were computed by synthesizing a homogeneous old stellar population for ages of 8 Gyr (triangles), 12 Gyr (squares), and 17 Gyr (small asterisks); metallicity decreases along each model sequence, from top to bottom, from +0.5 to –0.5 dex. The symbols connected by dashed lines represent observational data for the circumnuclear region of NGC 4036: our May 1997 data (large circles connected in order of increasing distance from the center) and the data of Fisher *et al.* (1996) for the major (pluses) and minor (large asterisks) axes. We estimated the position of the NGC 4036 nucleus in this diagram (marked by nuc) by averaging the 1997 and 1998 MPFS data and the Nasmyth-1 data. The magnesium index was corrected for the [N I] λ5200 emission. The dots represent the central regions of moderate-luminosity (M_B = –19...–20) ellipticals, as deduced from the data of Trager *et al.* (1998).

Curious physical conclusions can be reached by examining the dependence Hβ(r). In contrast to similar radial metal-line profiles, the profiles of Fisher *et al.* (1996) for Hβ along the major and minor axes differ markedly (the azimuthally averaged dependences lie between them). The most natural explanation is that the ionized gas concentrated into a fairly thin disk, i.e., visible predominantly along the major axis, floods the absorption more heavily precisely in this profile. If the deviation of the Hβ profile along the major axis from that along the minor one is taken to be a measure of the Balmer-emission intensity, then we conclude that the hydrogen emission, together with, possibly, star-forming regions, exhibits a flat ring-shaped distribution with a ~2″.5 radius. This is the same Hα ring as that found by Pogge and Eskridge (1993) at the centers of the lenticular galaxies NGC 4138 and 7013; however, they could not find it in NGC 4036, because the hydrogen emission here is lost in the intense Balmer absorption. At $R \geq 5''$, the difference between the Hβ-index profiles along the major and minor axes vanishes.

Unfortunately, the fact that the Hβ absorption line is flooded with emission prevents us from using a comparison of Hβ and Mgb or Hβ and ⟨Fe⟩ ≡ (Fe5270+Fe5335)/2 to separate the age and metallicity effects and to accurately determine each of the parameters. However, the (⟨Fe⟩, Mgb) diagram (Fig. 2) shows the NGC 4036 nucleus to be chemically decoupled. In this diagram, all models with a solar magnesium-to-iron ratio, irrespective of their common metallicity and star-formation history, are located within a narrow sequence, while any deviations from this sequence can be interpreted only as a nonsolar Mg/Fe ratio. Before transferring the data from Fig. 1 to the (⟨Fe⟩, Mgb) diagram (Fig. 2), we corrected the measured magnesium index for the [N I] λ5200 emission, which is rather strong at the NGC 4036 center. As Goudfrooij and Emsellem (1996) showed, the [N I] λ5200 emission line falls within the wavelength range where the continuum for the magnesium index is measured, and the presence of emission thus artificially increases its value; the correction that they recommend to apply to the magnesium index is approximately equal to 1.13EW([N I]). The data for NGC 4036 within a 5″ radius in Fig. 2 were corrected for the [N I] emission according to these recommendations. We can now directly estimate Mg/Fe for the stellar population. We see from Fig. 2 that the NGC 4036 nucleus is distinguished by an enhanced magnesium-to-iron ratio. This peculiarity is most likely characteristic of the stellar populations in ellipticals (Worthey *et al.* 1992), and we plotted the data from Trager *et al.* (1998) for the central regions of medium-luminosity ellipticals (M_B = –19…–20) in Fig. 2 for comparison: the NGC 4036 nucleus fell just in the middle of this cloud of data points. Based on the model of Tantalo *et al.* (1998), we estimated [Mg/Fe] for the NGC 4036 nucleus to be +0.3; Jablonka *et al.* (1996) obtained [Mg/Fe] ≈ +0.4 from their integrated measurements through a 10″.5 × 2″.5 aperture. We believe this estimate to refer primarily to the nucleus as being considerably brighter than the nearby portions of the bulge. What distinguished NGC 4036 from most ellipticals is that the Mg/Fe ratio abruptly changes when passing from the nucleus to the bulge. As Worthey *et al.* (1992) showed, the elemental abundances in ellipticals change radially in such a way that the galaxy displaces in the (⟨Fe⟩, Mgb) diagram almost parallel to the model sequence [Mg/Fe] = 0; i.e., Mg/Fe remains radially constant. At the same time, the Mg/Fe ratio in NGC 4036 (Fig. 2) clearly drops when passing from the nucleus to the bulge: [Mg/Fe] ≈ +0.1 as inferred from our data, while it is nearly solar as inferred from the data of Fisher *et al.* (1996). Since theoreticians of the chemical evolution of galaxies associate the Mg/Fe ratio primarily with the duration of the epoch of main star formation in stellar systems, we can state that the histories of star formation in the nucleus and bulge of the lenticular galaxy NGC 4036 were different.

STRUCTURE OF THE CENTRAL REGION IN NGC 4036

The galaxy NGC 4036 has a rich history of photometric studies. First Barbon *et al.* (1978) analyzed a two-dimensional photographic *B*-band image of the galaxy in detail and found it to consist of a bulge and an extended disk, which begins to dominate even at $R \approx 20''$ (2.1 kpc). They measured the following morphological parameters: the galaxy inclination, $i = 71°$, and the position angle of the isophotal major axis, $PA_0 = 79°$ (we included their data in Table 1). CCD observations followed next: Kent (1984, 1985) measured the radial variations in morphological parameters in outer regions and separated the disk and the bulge in the red filter *r*. Michard and Marchal (1993) measured the variations in morphological parameters with radius in its complete range at a moderate spatial resolution of 2″.6–2″.8 and found the *B* and *V* isophotes at $R < 10''$ to be moderately box-shaped. Finally, Cinzano *et al.* (1999) again performed complete *V*-band surface photometry of NGC 4036 with the 2.3-m Bok ground-based telescope (KPNO) with a spatial resolution of 1″.7 and on the basis of HST data with 0″.1 resolution through an F547M filter, which we also use below (see the next section). All these published data remarkably agree with each other, suggesting that the peculiarities of the central structure of NGC 4036 have been firmly established; nevertheless, they have avoided a detailed discussion so far. We rely primarily on the most recent study by Cinzano *et al.* (1999); previous studies are consistent with it, but have a lower spatial resolution.

First of all, Cinzano *et al.* (1999) note an appreciable turn of the isophotal major axis from PA = 98° at $R = 1''$ to PA = 67° at $R = 5''$: the ellipses, as it were, oscillate about the location of the line of nodes for the global disk $PA_0 = 79°$. An equilibrium orientation is reached at $R \approx 10''$ and does not change any longer further out. According to ground-based observations, the isophotal ellipticity does not tend to zero as the center is approached, as is usually the case in galaxies with big bulges; it freezes at ~0.12. As regards the HST data with their excellent resolution, they reveal a local maximum $1 - b/a \approx 0.3$ at $R \approx 2''$. Cinzano *et al.* (1999) propose to explain such a behavior of the isophotes at the NGC 4036 center in two possible ways: either this is an intricate dust distribution which seems to them to be more likely, or this is a manifestation of a "slight triaxiality" of the inner bulge regions. Given that the fourth coefficient a_4 of the cosine of an azimuthal Fourier decomposition of the brightness at $R = 1''$ is approximately equal to $+0.01a$, we can offer a third plausible explanation: there is a tilted circumnuclear stellar disk at the NGC 4036 center; in that case, however, the nature of the deviation of the isophotal major axis from the line of nodes at $R = 3''$–$5''$ is yet to be elucidated. One of these three hypotheses can be chosen only by simultaneously analyzing photometry and kinematics (see the next section).

It is also curious to compare the ionized-gas distribution at the NGC 4036 center with the distribution of stars. Based on the intensity profile of the [OII] λ3727 emission line (the slit was placed along the major axis), Cinzano *et al.* (1999) assure that the emission-line intensity profile within $R < 6''$ follows de Vaucoulers' law. Since the velocity dispersion of gas clouds within $R < 5''$ also increases sharply, it is immediately concluded that the gas at the very center of NGC 4036 closely follows the distribution and kinematics of stars and most likely has its origin in stellar winds from bulge red giants. The kinematics is discussed in the next section, while Fig. 3a shows a two-dimensional intensity distribution of the [N II] λ6583 emission line in comparison with the intensity in the neighboring continuum, which characterizes the distribution of old stars. The distributions are seen to be different: intensity isophotes of the [N II] emission line appear more elongated than do continuum isophotes. Figure 3b shows the radial variations in major-axis position angle and in isophotal ellipticity of both distributions calculated by using the FITELL code. In general, the quantitative morphological parameters deduced from MPFS images should have been treated with caution: the number of independent image elements is too small, while the point spread function is a moderately circular two-dimensional Gaussian. However, we can check the accuracy of PA and $1 - b/a$ calculated in our specific case by comparison, for example, with the results of Michard and Marchal (1993): their *B*-band observations were carried out at 2″.65 seeing, almost as in our case. This comparison (Fig. 3b) indicates that our results pertaining to continuum isophotes are very close to reality: the ellipticities just match closely, while the radial variations in position angle are repeated with a small systematic shift. Based on Fig. 3b, we can there-

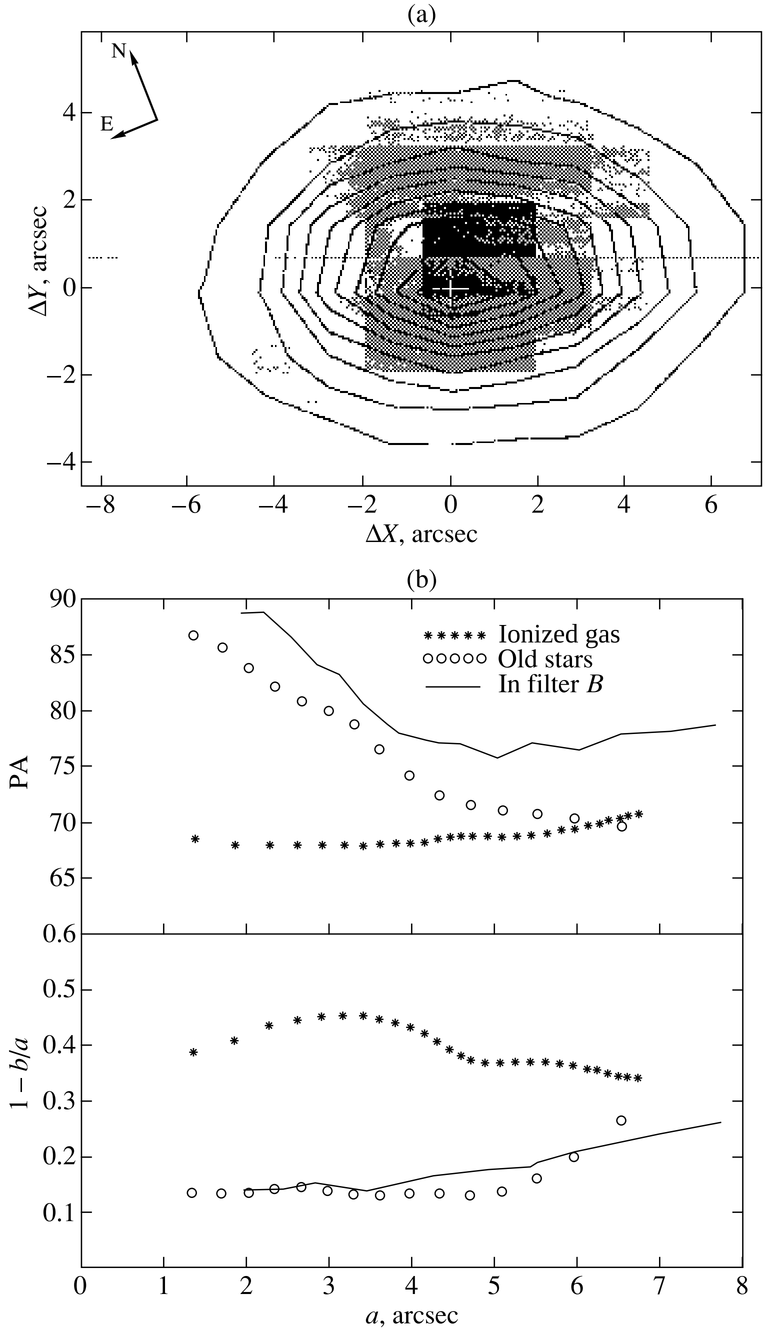

Fig. 3. Comparison of morphological parameters for the distribution of ionized gas and stars at the NGC 4036 center, as deduced from our MPFS data in the spectral range 6200–6900 Å: (a) surface-brightness isophotes for the continuum at 6500 Å (filled) and for the [N II] λ6583 Å emission line (contour); and (b) radial variations in the position angle of the major axis of isophotes and in their ellipticity, as inferred from our MPFS data in continuum (circles) and in the [N II] emission line (asterisks), as well as from the *B*-band data of Michard and Marchal (1993) at a seeing similar to ours.

fore assert with confidence that Cinzano *et al.* (1999) are wrong, and that the ionized-gas distribution at the NGC 4036 center does not closely follow the distribution of stars at all. The major axes of the emission-line and continuum isophotes at $R = 1''$–$2''$ differ in position angle by almost 20°: the gas distribution up to the very center maintains an isophotal position angle PA ≈ 70°, to which the distribution of stars comes only at $R \approx 5''$. This result is also indirectly confirmed by the image from the HST archive. Figure 4 shows a map of the residual brightness through the F547M filter after the subtraction of a model image with regular elliptical isophotes whose parameters were calculated from the original image by means of the FITELL code. We see

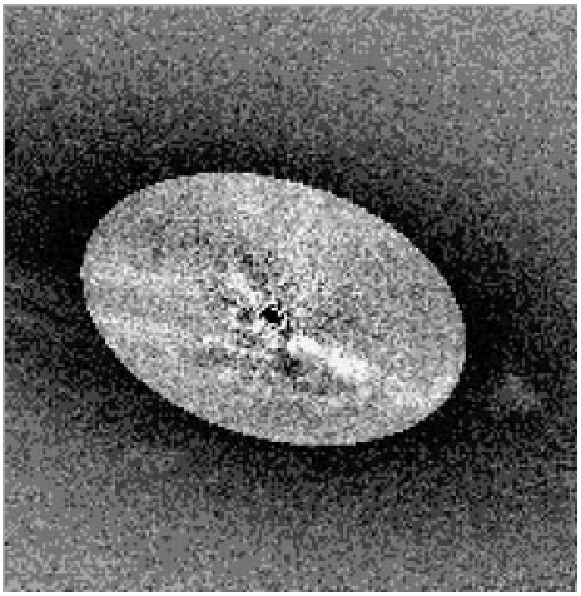

Fig. 4. A map of residual brightness through the F547M (WPFC2 HST) filter after subtracting a model with elliptical isophotes. North is at the top (vertical position angle +7°.5), and east is on the left; the imaged region is 34″ × 34″ in size. Since the model was not subtracted at the very center, it is painted black, and the light ellipse bounds the region in which the model was subtracted.

than the thin straight dust lane extends from the center to a distance of several arcsec just at PA ≈ 70°. In addition, the ellipticity of emission-line isophotes exceeds considerably the ellipticity of continuum isophotes, although it does not reach 0.6 typical of an infinitely thin disk tilted at 70° to the plane of the sky (as the global disk of NGC 4036). Thus, the gas at the NGC 4036 center is associated neither with the bulge nor with the global disk of the galaxy. Precisely what structure we see in the [N II] λ6583 emission can be determined by invoking kinematic data.

KINEMATICS OF THE GAS AND STARS IN THE CENTRAL REGION OF NGC 4036

The two-dimensional velocity fields of the stars and ionized gas constructed from our MPFS data are shown in Fig. 5. Basically, the two fields look very similar (at this spatial resolution), and both exhibit regular quasi-rigid rotation with approximately the same angular velocities. The lines of equal gas velocity show a faint hint of *z* distortion, which is usually characteristic of gas rotation in a triaxial potential. A local extremum at 7″ from the center fell with the measured portion of the stellar velocity field; otherwise, a more classical

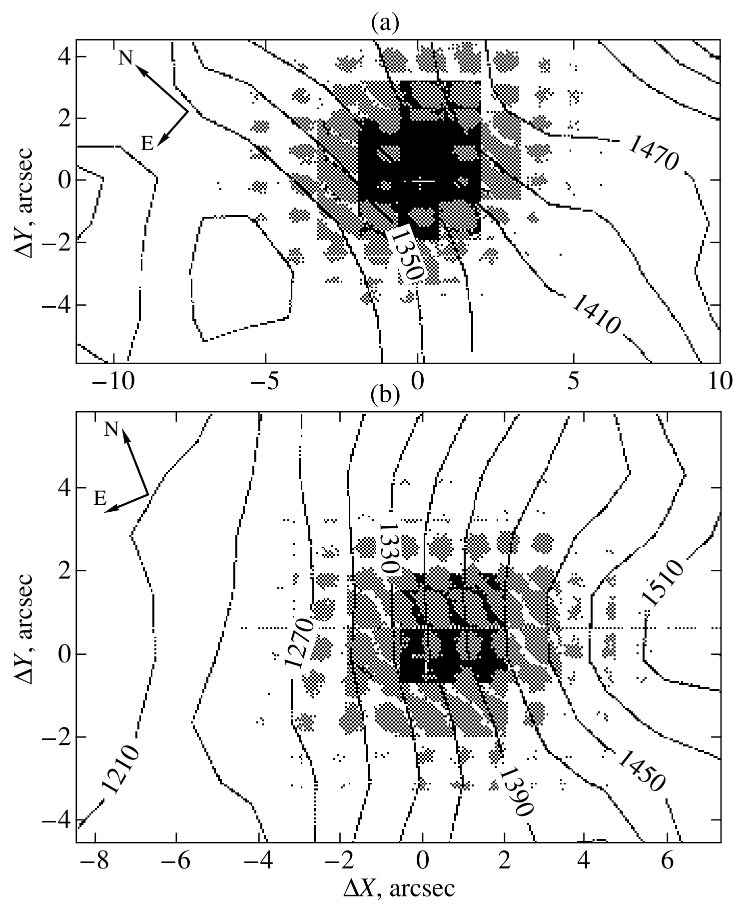

Fig. 5. Two-dimensional line-of sight velocity fields for (a) the stars and (b) ionized gas at the NGC 4036 center, as constructed from our MPFS data.

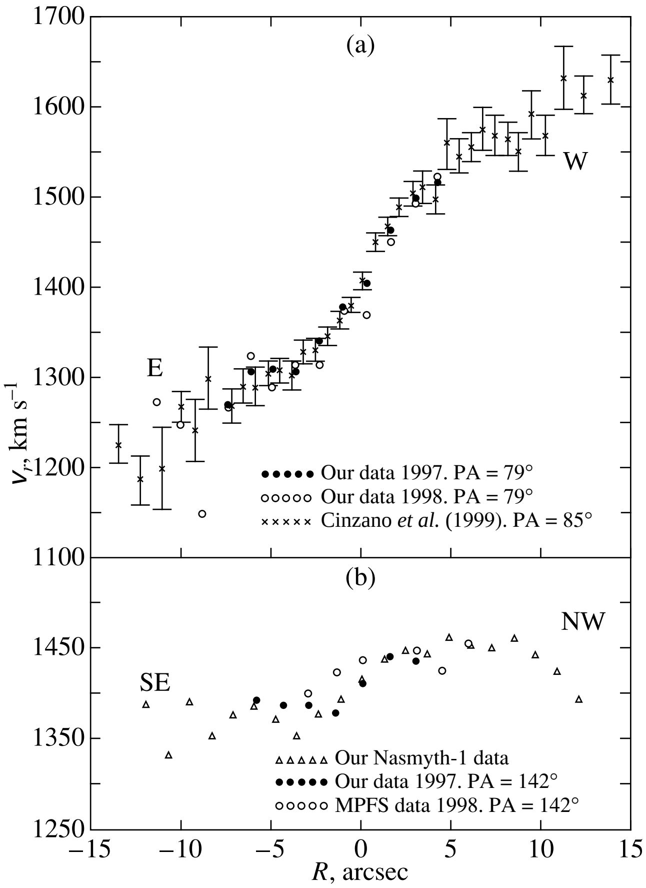

Fig. 6. Comparison of one-dimensional line-of-sight velocity profiles for the stellar component at the NGC 4036 center: (a) along the major axis; and (b) at 63° to the major axis.

appearance of the velocity field for circular rotation is difficult to imagine.

The quality of our gas and stellar line-of-sight velocity fields for the NGC 4036 center can be checked by comparing our data with published ones. However, the two-dimensional velocity fields have been obtained for NGC 4036 for the first time: only one-dimensional profiles constructed from long-slit observations can be found in the literature. We modeled such profiles using our data by superimposing narrow, 2″-wide masks oriented along the major axis on two-dimensional velocity fields. The model profiles are compared with the observational data of Cinzano *et al.* (1999) in Figs. 6 (stars) and 7 (ionized gas). Apart from a comparison of the velocity profiles along the major axis, Fig. 6 compares the line-of-sight velocity profiles of stars at 63° to the major axis: the model one and that constructed from our observations with the spectrophotometric system at Nasmyth-1. A joint analysis of the two parts of Fig. 6 indicates that the 1997 kinematic data are better than the 1998 data for stars; the May 1997 model profiles closely coincided with the slit ones. As regards the MPFS kinematic data for the ionized gas, they generally follow the profile of Cinzano *et al.* (1999), although they do not closely follow fine features such as the "steps" at $R = \pm 3''$–$5''$ or the counterrotating portion at the center. Clearly, this is because the spatial resolution of our 1998 observations was approximately a factor of 2 lower than that for the observations of Cinzano *et al.* (1999). On the other hand, the two-dimensional line-of-sight velocity distributions allow us to diagnose the pattern of rotation and the axial symmetry of the potential, which cannot be done using a single profile along the major axis.

Under conditions of axisymmetric rotation, the azimuthal variations in apparent central line-of-sight velocity gradient obey a cosine law as long as we remain within the region of rigid rotation:

$$dv_r/dr = \omega \sin i \cos(\mathrm{PA} - \mathrm{PA}_0),$$

where ω is the angular velocity of the galactic center, i is the inclination of the galaxy's disk rotation axis to the line of sight, and PA_0 is the position angle of the line of nodes. In NGC 4036, the rotation is strictly rigid up to $R = 4''$ and virtually rigid up to $R \approx 8''$ (Fig. 6). Therefore, using our two-dimensional velocity fields (Fig. 5), we determined the positions of maxima in the azimuthal dependences of central line-of-sight velocity gradients, which we call below the orientation of the dynamical major axis, both for stars and for the gas, at several distances from the center in the range $R = 1''.5$–$5''.5$. To this end, we fitted cosine curves to the observed dependences of gradients dv_r/dr measured in three R ranges by least squares. The coincidence of the photometric and dynamical major axes proves that the rotation is axisymmetric, while the photometric and dynamical axes in a triaxial potential turn in opposite directions from the line of nodes of the rotation plane (Monnet *et al.* 1992). Figure 8 compares the orientations of the dynamical and photometric major axes in the central part of NGC 4036; whereas the HST data show the true orientation of the potential shape at a given radius, the data of Michard and Marchal (1993) exhibit a smoothing of the true dependence PA(R) for observations at seeing $\mathrm{FWHM}_* = 2''.6$. We see that the change in dynamical major axis, both for stars and, in general, for the gas, qualitatively corresponds to the change in photometric major axis with radius. Since the accuracy of determining the cosinusoid phases dv_r/dr(PA) is 3°–5°, the deviation of the dynamical major axes of ionized-gas rotation from the line of nodes of the global galactic disk may actually turn out to be insignificant. However, a turn of the dynamical major axis through 20° appears quite reliable, and it is consistent with the behavior of the photometric major axis as inferred from the data of Michard and Marchal (1993). We therefore conclude that the rotation of stars at the NGC 4036 center appears axisymmetric at each individual radius, but it definitely does not take place in the galaxy's principal plane within $R < 2''.5$. If we use high-resolution photometry, i.e., the HST data, then two discrete structures show up. One is seen at $R = 1''–3''$, is elongated at PA ≈ 90°, and is probably a circumnuclear stellar disk. The other is seen at $R = 4''–6''$ and is elongated at PA ≈ 70°; its nature is less clear.

DISCUSSION

What does happen at the NGC 4036 center in the first place? Objecting to Cinzano *et al.* (1999), we can now say with confidence that the turn of the isophotal major axis through 30° within 5″ of the center is not merely the semblance due to a clumpy dust distribution, because the dynamical major axis of stars also exhibits a similar turn. Taking into account the coincidence of the photometric and dynamical major axes of the stellar component within $R \le 2''$, the positive parameter a_4, and the local ellipticity maximum at $R = 1''–2''.5$, we conclude that a tilted compact stellar disk with a radius of 250 pc most likely exists at the very center of NGC 4036. The nature of the structural component that manifests itself in morphology at $R = 3''–6''$ is less clear. On the one hand, this may also be a tilted (in the opposite direction) stellar disk. However, the isophotal ellipticity at this location is rather low. On the other hand, there are such puzzling features in NGC 4036 as the straight narrow dust lane at PA = 250°(70°), which extends from the nucleus westward (Fig. 4), and ionized-gas counterrotation within ±1″ of the nucleus (Fig. 7), which is seen in the kinematic profiles along the major axis obtained by Fisher (1997) and, independently, by Cinzano *et al.* (1999) (it did not manifest itself in our data because of insufficient spatial resolution). The dust lane at PA = 250° with no extension on the other side of the nucleus lies in the galaxy's half that recedes from us as it rotates and closely resembles a shock front in the gas striking the bar edge. The change in the sense of rotation of the gas, which is a dissipative component, as the galaxy center is approached would also be expected most likely in a triaxial potential, where there are intense radial flows and the tangential gas velocity is suppressed by the shock wave. It may well be that the compact bulge of NGC 4036, which, as follows from the decomposition of the radial brightness profile by Kent (1985) and Cinzano *et al.* (1999), dominates over the disk only within $R < 7''$, is actually triaxial, with the projected major axis at PA ≈ 70°. The constant isophotal orientation of the [N II] emission surface-brightness distribution, PA ≈ 70° (Fig. 3b), can then be explained by the fact that the gas "settled" to the principal plane of the triaxial bulge.

We have repeatedly pointed out a discrepancy between the sizes of chemically and structurally decoupled regions at the centers of early-type disk galaxies. There are simultaneously an unresolved chemically decoupled nucleus and much more extended (up to a radius of 100–800 pc) circumnuclear stellar disks in M 31 (Sil'chenko *et al.* 1998), NGC 4216 and 4501 (Sil'chenko *et al.* 1999), and the S0 galaxies NGC 1023

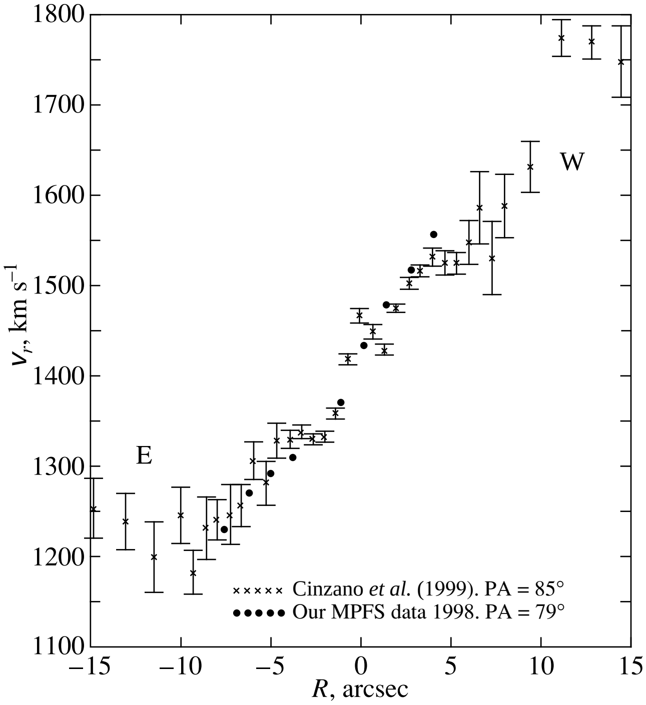

Fig. 7. Comparison of one-dimensional line-of-sight velocity profiles for the ionized gas at the NGC 4036 center; the slit is aligned with the major axis.

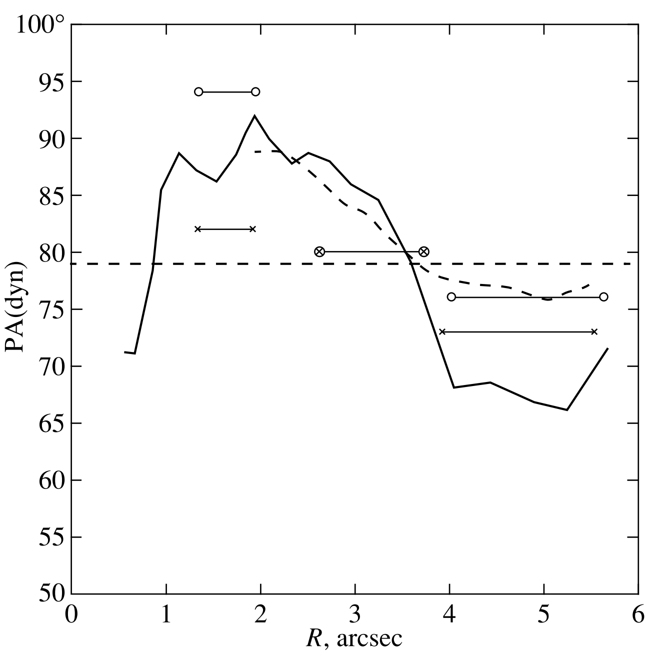

Fig. 8. Comparison of the orientations of the photometric major axis [the solid line and the line with short dashes represent the HST data and the data of Michard and Marchal (1993), respectively] and the dynamical major axis for the stars (the circles represent our 1997 MPFS data) and ionized gas (crosses). The horizontal line with long dashes specifies the orientation of the line of nodes for the global galactic disk.

and 7332 (Sil'chenko 1999a). In some cases, for example, in NGC 1023 (Sil'chenko 1999a) or NGC 7331 (Sil'chenko 1999b), we managed to firmly establish a difference in the ages of these subsystems: the mean ages of stars in the nucleus is 2 to 3 Gyr older than that in the circumnuclear disk; the nuclei exhibit a magnesium overabundance, while the Mg/Fe ratio in the disks is solar. All of this fits in a scenario where a secondary starburst in the nucleus and in the circumnuclear disk began quasi-simultaneously, but it ended much earlier in the nucleus and lasted for another 2 to 3 Gyr in a ring zone around the nucleus. Although the age of the stellar population at the NGC 4036 center has not yet been reliably determined, the abrupt change in Mg/Fe between the nucleus and its immediate vicinity, including the circumnuclear stellar disk, argues precisely for this scenario for this galaxy as well.

ACKNOWLEDGMENTS

We wish to thank A.N. Burenkov and S.N. Dodonov from the SAO, as well as A.V. Moiseev, a postgraduate at the SAO, for help with the 6-m telescope observations. The observational data used here were obtained with the 6-m telescope financed by the Ministry of Science of the Russian Federation (register number 01-43) and with the NASA/ESA Hubble Space Telescope operated by the Association of Universities for Studies in Astronomy under contract with the NASA (NAS 5-26 555). We used data from the HST archive. We also used the LEDA database, provided by the LEDA team at the CRAL Lyon Observatory (France). This study was supported by the Russian Foundation for Basic Research (project no. 98-02-16196), the President's grant of the Russian Federation for support of Doctors of Science (no. 98-15-96029), and a grant of the Russian State Science and Technology Program "Astronomy. Fundamental Space Research" (Astronomy Section) 1.2.4.1.

REFERENCES

1. V. L. Afanasiev and O. K. Sil'chenko, Astron. J. **119**, 126 (2000).
2. V. L. Afanas'ev, V. V. Vlasyuk, S. N. Dodonov, and O. K. Sil'chenko, Preprint No. 54 (Special Astrophysical Observatory, 1990).
3. R. Barbon, L. Benacchio, and M. Capaccioli, Astron. Astrophys. **65**, 165 (1978).
4. F. Bertola, L. M. Buson, and W. W. Zeilinger, Astrophys. J. Lett. **401**, L79 (1992).
5. F. Bertola, P. Cinzano, E. M. Corsini, *et al.*, Astrophys. J. Lett. **448**, L13 (1995).
6. P. Chamaraux, C. Balkowski, and P. Fontanelli, Astron. Astrophys. **165**, 15 (1986).
7. P. Cinzano, H.-W. Rix, M. Sarzi, *et al.*, Mon. Not. R. Astron. Soc. **307**, 433 (1999).
8. D. Fisher, Astron. J. **113**, 950 (1997).
9. D. Fisher, M. Franx, and G. Illingworth, Astrophys. J. **459**, 110 (1996).
10. P. Goudfrooij and E. Emsellem, Astron. Astrophys. **306**, L45 (1996).
11. W. K. Huchtmeier, Astron. Astrophys. **110**, 121 (1982).
12. P. Jablonka, P. Martin, and N. Arimoto, Astron. J. **112**, 1415 (1996).
13. S. M. Kent, Astrophys. J., Suppl. Ser. **56**, 105 (1984).
14. S. M. Kent, Astrophys. J., Suppl. Ser. **59**, 115 (1985).
15. R. Michard and J. Marchal, Astron. Astrophys., Suppl. Ser. **98**, 29 (1993).
16. G. Monnet, R. Bacon, and E. Emsellem, Astron. Astrophys. **253**, 366 (1992).
17. R. W. Pogge and P. B. Eskridge, Astron. J. **93**, 291 (1987).
18. R. W. Pogge and P. B. Eskridge, Astron. J. **106**, 1405 (1993).
19. M. S. Roberts, D. E. Hogg, J. N. Bregman, *et al.*, Astrophys. J. Suppl. Ser. **75**, 751 (1991).
20. W. Seifert and C. Scorza, Astron. Astrophys. **310**, 75 (1996).
21. O. K. Sil'chenko, Pis'ma Astron. Zh. **19**, 693 (1993) [Astron. Lett. **19**, 279 (1993)].
22. O. K. Sil'chenko, Astron. J. **117**, 2725 (1999a).
23. O. K. Sil'chenko, Astron. J. **118**, 186 (1999b).
24. O. K. Sil'chenko, V. L. Afanas'ev, and V. V. Vlasyuk, Astron. Zh. **69**, 1121 (1992) [Sov. Astron. **36**, 577 (1992)].
25. O. K. Sil'chenko, A. N. Burenkov, and V. V. Vlasyuk, Astron. Astrophys. **337**, 349 (1998).
26. O. K. Sil'chenko, A. N. Burenkov, and V. V. Vlasyuk, Astron. J. **117**, 826 (1999).
27. R. Tantalo, C. Chiosi, and A. Bressan, Astron. Astrophys. **333**, 419 (1998).
28. S. C. Trager, G. Worthey, S. M. Faber, *et al.*, Astrophys. J., Suppl. Ser. **116**, 1 (1998).
29. F. C. van den Bosch and E. Emsellem, Mon. Not. R. Astron. Soc. **298**, 267 (1998).
30. A. Vazdekis, E. Casuso, R. F. Peletier, and J. E. Beckman, Astrophys. J., Suppl. Ser. **106**, 307 (1996).
31. V. V. Vlasyuk, Izv. Spets. Astrofiz. Obs. **36**, 107 (1993).
32. G. Worthey, Astrophys. J., Suppl. Ser. **95**, 107 (1994).
33. G. Worthey, S. M. Faber, and J. J. González, Astrophys. J. **398**, 69 (1992).
34. G. Worthey, S. M. Faber, J. J. González, and D. Burstein, Astrophys. J., Suppl. Ser. **94**, 687 (1994).

Translated by V. Astakhov